DOI: 10.1161/CIRCULATIONAHA.114.015036

Coordinated Membrane Ballooning and Procoagulant-Spreading in Human Platelets

Running title: *Agbani et al.; Ballooned and Procoagulant-Spread Platelets*

Ejaife O. Agbani, BPharm, MSc, PhD[1]; Marion T.J. van den Bosch, BSc, MSc, PhD[1]; Ed Brown, BSc, PhD[1]; Christopher M. Williams, BSc, PhD[1]; Nadine J.A. Mattheij, BSc, MSc, PhD[2]; Judith M.E.M Cosemans, BSc, MSc, PhD[2]; Peter W. Collins, MD, PhD[3]; Johan W.M. Heemskerk, BSc, MSc, PhD[2]; Ingeborg Hers, BSc, MSc, PhD[1*]; Alastair W. Poole, MA, PhD, VetMB[1*]

[1]School of Physiology & Pharmacology, University of Bristol, Bristol, United Kingdom; [2]Dept of Biochemistry, Cardiovascular Research Institute Maastricht (CARIM), University of Maastricht, Maastricht, the Netherlands; [3]Welsh Blood Service and Arthur Bloom Haemophilia Centre, School of Medicine, Cardiff University, Cardiff, United Kingdom

*Co-senior authors

Address for Correspondence:

Alastair W. Poole, MA, PhD, VetMB and Ejaife O. Agbani, BPharm, MSc, PhD

School of Physiology & Pharmacology, Bristol Cardiovascular, Bristol Platelet Group

University of Bristol, Medical Sciences Building

University Walk, Bristol, BS8 1TD

United Kingdom

Tel: + 44 117 331 1435

Fax: + 44 117 331 2288.

E-mail: a.poole@bristol.ac.uk and e.agbani@bristol.ac.uk

Journal Subject Codes: [97] Other vascular biology, [179] Morphology, [181] Signal transduction, [176] Thrombin, [92] Platelets

DOI: 10.1161/CIRCULATIONAHA.114.015036

Abstract

Background—Platelets are central to the process of haemostasis, rapidly aggregating at sites of blood vessel injury and acting as coagulation nidus sites. Upon interaction with sub-endothelial matrix platelets are transformed into balloon-like structures as part of the haemostatic response. It remains unclear, however, how and why platelets generate these structures. We set out to determine the physiological relevance and cellular and molecular mechanisms underlying platelet membrane ballooning.

Methods and Results—Using 4D live-cell imaging and electron microscopy, we show that human platelets adherent to collagen are transformed into phosphatidylserine-exposing balloon-like structures with expansive macro/micro-vesiculate contact surfaces, by a process which we termed procoagulant-spreading. We reveal that ballooning is mechanistically and structurally distinct from membrane blebbing and involves disruption to the platelet microtubule cytoskeleton and inflation through fluid entry. Unlike blebbing, procoagulant ballooning is irreversible and a consequence of Na^+, Cl^- and water entry. Furthermore, membrane ballooning correlated with micro-particle generation. Inhibition of Na^+, Cl^- or water entry impaired ballooning, procoagulant-spreading, micro-particle generation and also diminished local thrombin generation. Human Scott syndrome platelets, which lack expression of Ano-6, also showed a marked reduction in membrane ballooning, consistent with a role for chloride entry in the process. Finally, blockade of water entry by acetazolamide attenuated ballooning in vitro, and markedly suppressed thrombus formation *in vivo* in a mouse model of thrombosis.

Conclusions—Ballooning and procoagulant-spreading of platelets are driven by fluid entry into the cells, and are important for amplification of localised coagulation in thrombosis.

Key words: cell physiology; hemostasis; coagulation; platelet; collagen; membrane ballooning; procoagulant-spreading; microparticles; fluorescent imaging; high-resolution microscopy

DOI: 10.1161/CIRCULATIONAHA.114.015036

Introduction

Platelets play complex roles in haemostasis and arterial thrombosis, rapidly adhering to sub-endothelial structures and to each other to generate a platelet aggregate which is stabilised by the local production of thrombin and subsequently fibrin[1]. Critical to this response is the surface exposure of aminophospholipids, particularly phosphatidylserine (PS), which promotes assembly of the tenase and prothrombinase complexes on the platelet surface. This platelet-dependent procoagulant activity therefore depends upon two major factors: (i) the degree of PS exposure and (ii) the surface area of membrane with exposed PS.

It is currently thought that a sustained rise in cytosolic Ca^{2+} is required for exposure of PS on the extracellular leaflet of the plasma membrane, through activation of a non-specific phospholipid scramblase and inhibition of a PS translocase or flippase. Anoctamin-6 (gene *ANO6 or TMEM16F*) is identified as a key regulator of calcium-dependent PS exposure[2], and loss-of-function mutations in anoctamin-6 have been shown in two Scott syndrome patients[3, 4], who have aberrant calcium-dependent scramblase activity[5]. However the precise role played by anoctamin-6 is still unclear. It is possible that, like other members of the anoctamin family, it forms Ca^{2+}-activated Cl^- channels[6]. Although much effort has gone into determining the molecular mechanisms regulating surface PS exposure, relatively little is known about the mechanisms by which platelet membrane surface area may be maximised. Possibly, Cl^- entry may also be required for a change in membrane surface area, and this would be another distinct functional role for Cl^- entry in potentiating platelet procoagulant activity.

Platelets have long been reported to transform *in vivo* to form balloons upon activation, and fibrin has been shown to fill the space between these balloon structures at wound sites[7-9]. Platelet membrane ballooning has also been observed *in vitro* in platelets adherent to

immobilised collagen[10-12]. However, it is not clear whether this striking morphological change is analogous to apoptotic blebbing in other cell types[13-15]. Attempts to assess ballooning in platelets have been limited by the methods of investigation, imaging resolution[10] and the fragility of the balloon structure which often results in its loss or significant deformation[11].

Here we hypothesised that platelet ballooning was important to markedly increase the surface area of exposed membrane, and exposed PS, thereby enhancing the local procoagulant response[10, 16, 17]. We used detailed dynamic imaging approaches to visualise thrombin generation on platelet membrane surfaces and to understand the mechanisms regulating ballooning. This study revealed that the key mechanism involves fluid entry, accompanied by the genesis of a novel spread membrane structure in a process we have termed 'procoagulant-spreading'. Unlike conventional lamellipodial spreading, this form of spreading yields procoagulant surfaces, and rapidly breaks up by multiple coalescences to form numerous procoagulant microvesicles. Ballooning and procoagulant-spreading are therefore linked processes which are likely to contribute to hemostatic responses *in vivo*.

Methods

Written informed consent was obtained in accordance with the Declaration of Helsinki.

Human blood was obtained from healthy drug-free volunteers under Local Research Ethics approval (E5736). The UK Scott patient blood was obtained with NHS Research Ethics Committee approval, and has been described. This Scott patient is a compound *TMEM16F* heterozygote, IVS6 + 1G→A, resulting in exon 6 skipping. Another mutation in this patient, (c.1219insT) causes premature translation termination and defective expression of TMEM16F[4, 18].

Materials

Details of materials used are given in Supplementary files.

DOI: 10.1161/CIRCULATIONAHA.114.015036

Platelet-rich plasma preparation

Blood drawn from healthy human volunteers was anticoagulated with 0.4% trisodium citrate and acidified with 16% acid citrate dextrose (85 mmol/L trisodium citrate, 71 mmol/L citric acid, 111 mmol/L glucose). Platelet-rich plasma (PRP) was obtained by centrifugation at 180 *g* for 17 min.

Washed human platelet preparation

PRP was centrifuged at 650 *g* for 10 min in the presence of 10 μmol/L indomethacin and 0.02 U/mL apyrase, and resuspended in HEPES-Tyrode's buffer modified with 0.1% (w/v) glucose, 10 μmol/L indomethacin, and 0.02 U/mL apyrase. Sodium and chloride free HEPES-Tyrode's buffers were prepared by replacing Na^+ and Cl^- with equimolar N-methyl-D glucamine and gluconate, respectively.

Live cell confocal microscopy

Washed human platelets were pre-incubated (10 minutes) with calcium dye Fluo-4 AM and Alexa Fluor 568 annexin-V conjugate (1%$^{V}/_{V}$). Hyperosmolar Tyrodes' was prepared by adding 40 mmol/L sucrose to HEPES-Tyrode's buffer. MatTek dishes were pre-coated with collagen (20 μg/mL) and aliquots of platelet suspensions were added ($2x10^7$ cells/mL), supplemented with 1 mmol/L $CaCl_2$. Changes in relative fluorescence intensity (F/F_0) over time were monitored. Details of confocal microscopy are given in Supplementary files.

Measurement of platelet thrombin generation

PRP was incubated with fluorogenic thrombin substrate, Z-GGR-AMC (450 μmol/L). PRP was re-calcified and thrombin generation initiated with 5 pmol/L tissue factor. Thrombin substrate was measured on platelet membrane surfaces and traces for single platelets and platelet aggregates were converted into first-derivative curves.

DOI: 10.1161/CIRCULATIONAHA.114.015036

Image deconvolution and analysis

Raw intensities from time-series (single plane over time) images were quantified after regions of interest were chosen and images corrected for background noise. For each platelet analysed, relative fluorescence (F/F_0) is reported; where F_0 designates the background-subtracted fluorescence level before platelet activation. Deconvolution of Z-stack images was based on calculated point spread functions; 3D & 4D reconstruction, movie rendering and co-localisation analysis were performed using Volocity imaging software (Perkin-Elmer, UK).

In vitro and *in vivo* thrombosis assays

Details of in vitro and in vivo thrombosis assays are given in Supplementary files.

Statistical analysis

Data were analyzed using GraphPad Prism 6 (San Diego, CA) and presented as interleaved box plots with whiskers showing min to max values and interquartile ranges. We determined statistical significance by the Friedman test, followed by Dunn's multiple comparison test or by Wilcoxon Signed Rank Test. $p<0.05$ (*) or $p<0.01$ (**) was considered significant.

Results

Spatiotemporal dynamics of platelet membrane ballooning and phosphatidylserine exposure

Upon interaction with sub-endothelial matrix platelets are transformed into balloon-like structures as part of the haemostatic response[7-10]. To obtain more temporal and dynamic insight into platelet ballooning, we used phase-contrast and confocal live cell imaging microscopy techniques to study platelet adhesion and ballooning on a collagen-coated surface. In the early phases of contact with collagen, platelets formed small, retractable membrane blebs (**Figure 1A**, image 2-7, blue arrows).

However, in many platelets, one of these blebs can swell to become a balloon (**Figure 1A**, image 10, yellow arrow), which ranged between 1 - 6 μm in diameter and typically did not retract (**Figure 1A**, **Movie S1**). We identified three distinct phases leading to balloon formation, which we termed phases Ph_1, Ph_2 and Ph_3 (**Figure 1B**). Ph_1 was characterised by blebbing (membrane protrusion ≤ 1 μm) (**Figure 1A and B**, images 1-5). During Ph_2, the membrane of non-retracted blebs rapidly expanded (images 6-8) and in Ph_3, the expansion plateaued (images 9-10). Initiation of ballooning was typically by 5 min after adhesion of the platelet to collagen fibre, and progressed rapidly to phase 3 by a further 5 min. Importantly, we observed platelet ballooning *in vivo*, in a mouse thrombus formation model (**Figure S1A**), consistent with previous observations[7-9]. Ballooning also occurred in human thrombi, as shown in *in vitro* flow studies (**Figure S1B, C**). Interestingly there was no ballooning in platelets adherent to von Willebrand factor in the presence of botrocetin, suggesting agonist specificity of the response.

A 3D recontruction showed that the platelet body and the balloon membrane bound labelled annexin-V, demonstrating PS exposure and generation of a procoagulant surface[5, 19-21] (**Figure 1C**, **Movie S2**). Annexin-V binding was characterised by two stages: Initially, a low level (F/F_0 = 1.3-1.5) of annexin-V accumulated on the membrane of the platelet body alone (**Figure 1D**, images 1-5), followed by annexin-V binding to the balloon as well (**Figure 1D**, images 7-10, **Movie S3**). Importantly, PS externalisation did not temporally correspond with membrane ballooning (**Figure 1E&F**), suggesting a distinction between the mechanisms underlying these two events. Furthermore, integrin $\alpha_{IIb}\beta_3$ was activated at an early time point prior to ballooning, but was sustained and localised just to the platelet body (**Figure 1G, H**).

Thrombin is generated on the ballooned surface of human platelets adherent to collagen

To demonstrate that ballooned platelets support a procoagulant response, we visualised the

formation of thrombin using the fluorogenic thrombin substrate Z-Gly-Gly-Arg aminomethyl coumarin (ZGGR-AMC, **Figure 2Ai**, cyan blue). 3D reconstruction further confirmed that thrombin was generated all over the balloon and platelet body (**Figure 2Aii**). **Figure 2Aiii** shows that thrombin is generated within 300-450 sec after platelet adhesion to collagen. This strongly correlated with balloon formation and annexin-V binding by single platelets (compare with **Figure 1B and E, F**).

Platelets from patients with Scott syndrome show significantly impaired PS exposure and procoagulant activity[18]. Here we show that platelets from the UK Scott syndrome patient have a marked defect in balloon formation compared to control platelets (**Figure 2B**, see arrows). Platelet ballooning may therefore be important for the procoagulant response, by increasing the available surface area for recruitment of the tenase and prothrombinase complexes (**Figure S2**).

Ballooned and procoagulant-spread (BAPS) platelets

Using 4D imaging, we observed four distinct platelet phenotypes adherent to collagen (**Figure 3A**): (1) conventionally spread non-ballooned platelets (CSNB, annexin-V^-), (2) ballooned and procoagulant-spread platelets (BAPS, annexin-V^+), (3) ballooned non-spread platelets (BNS, annexin-V^+) and (4) non-ballooned and non-spread platelets (NBNS). The NBNS phenotype was typically annexin-V^- but could be induced to expose PS with prolonged stimulation. Procoagulant-spreading, in BAPS platelets, was only clearly identifiable by visualising annexin-V just above (between 0 and 0.75 μm) the collagen-coated surface (**Figure 3A&B**, in red, **Movie S4**). The area covered by procoagulant-spread platelets is generally much greater than by conventionally spread platelets and can extend to around 20 μm (**Figure 3A**). BAPS platelets constitute a distinct subpopulation of adherent platelets, and this report is the first characterisation of these structures.

Ballooning and procoagulant-spreading are synchronised events

4D live-cell imaging showed balloon formation started within 4 min after platelet adhesion and reached a maximal diameter by 9-10 min, as visualised by annexin-V binding (**Figure 4A&B**). Procoagulant membrane spreading followed membrane ballooning after a 1-2 min delay (**Figure 4A-Ci**) and both were temporally correlated (**Figure 4Ci**, **Movies S5&S6**). Only a small proportion of platelets (approx. 10%) ballooned without procoagulant-spreading (BNS; **Figure 4Cii**), and we did not observe procoagulant-spreading without ballooning These data suggest that ballooning is likely to be required for procoagulant-spreading, but not vice versa. In this experiment, after adhesion of platelets to collagen for 1 hr, the mean relative proportions of platelets were CSNB (27.4%), BNS (10.4%), BAPS (50.0%), NBNS AnxV$^-$ (5.9%), and NBNS AnxV$^+$ (6.3%) (**Figure 4Cii**).

BAPS platelets showed a punctate or cobble-stone annexin-V staining pattern (**Figure 4A&B**). In addition, BAPS platelets released microvesicles in a time-dependent manner (**Suppl. Figure S3**) and scanning electron microscopy showed the cobble-stone appearance to be microvesicles formed from BAPS platelets after 1 h adhesion (**Figure 4D-F**). This was clearly distinct from the CSNB platelet (**Figure 4E**). We therefore suggest that procoagulant-spreading forms the basis for microvesicle formation and release upon adhesion of platelets to surfaces.

Inhibition of actomyosin promotes membrane ballooning whilst blocking procoagulant-spreading

To determine the role of the actin cytoskeleton in ballooning and procoagulant-spreading, platelets were incubated with modulators of actin polymerisation or myosin motor activity. **Figure 5A** shows representative figures of annexin-V binding to platelets adhered to collagen in the presence of these inhibitors. Blebbistatin, which blocks myosin-II ATPase activity[22],

significantly promoted the progression of platelets ballooning and increased balloon diameter at Ph_3 (**Figure 5Aii**, **Figure S3**). Similar results were found with platelets pre-treated with cytochalasin-D or Y27632. However, whilst enhancing ballooning, blebbistatin, cytochalasin-D and Y27632 inhibited spreading, and therefore formation of the BAPS morphology, so that platelets were restricted to the BNS phenotype (**Figure 5Aii**). Platelets treated with jasplakinolide, to promote actin polymerisation[23], did not show any membrane ballooning or spreading. The data indicate that actin polymerisation and myosin contraction negatively control membrane ballooning. Inhibition of procoagulant-spreading using cytochalasin D also resulted in diminished thrombin generation (**Figure 5B**).

Probing live platelets with AlexaFluor-350 phalloidin showed staining in the spread membranes of BAPS platelets (**Figure 5C**), indicating that their membrane integrity was likely to be compromised and that the balloons were actin-rich (see also **Movie S7**). In contrast, CSNB platelets were phalloidin negative.

Platelet ballooning involves microtubule disruption at the exit point of the protrusion

Transmission electron microscopy images of platelets in the expansion phase (Ph_2) of ballooning revealed a neck structure that delineated the balloon from the main platelet body (**Figure S4A**; yellow arrows), beneath which lay a disrupted microtubule ring structure, shown in detail by TEM tomography (**Figure S4Aiii**, green arrows; **Movie S8**). Significantly, there was no microtubule architecture present in Ph_3 balloons (**Figure S4B**). In the later phases of balloon formation, the integrity of the membrane becomes compromised, since it becomes leaky to two low molecular weight dyes, calcein and propidium iodide (data not shown).

Platelet ballooning and procoagulant-spreading requires salt and water entry

The rapid growth of the platelet balloon suggested that it may be driven by fluid entry. Our data

showed a 1.6 ± 0.02 fold increase in $[Cl^-]_{cyt}$ after 5 min contact with collagen (**Figure 6A&B**), which was absent in Cl^- free medium (not shown). In similar experiments, we recorded transient Na^+ entry during platelet adherence to collagen (**Figure 6C&D**), which was absent in Na^+ free medium (not shown). The percentage of adhered platelets that ballooned (**Figure 6E**) and underwent procoagulant-spreading (BAPS, **Figure 6F**) was significantly attenuated in media lacking Cl^- or Na^+ ions. Interestingly, the peak change and half-life of annexin-V binding were significantly reduced under these conditions (**Figure S3**). It is likely that Cl^- entry was substantially mediated by calcium-activated chloride channels (CaCC) since the inhibitor of these channels, CaCCinh-A01, induced similar effects to removal of extracellular Cl^- (**Figure 6E and F**).

To assess whether water entry was required for ballooning, we increased extracellular osmolality, using sucrose, by 40 mmol/L, which significantly attenuated both ballooning (**Figure 7A**) and procoagulant spreading (BAPS, **Figure 7B**), but not blebbing (**Figure 7A**). Furthermore, mean balloon diameter was attenuated in the small proportion of platelets able to balloon (**Figure S3A**). Acetazolamide has been shown to block aquaporin water channels[24], and it induced a characteristic retraction of the ballooning membrane (**Figure 7A**) and attenuated membrane accumulation of annexin-V (**Movie S9**). Importantly, there was also a marked reduction in formation of BAPS platelets (**Figure 7B**), suggesting a requirement for water entry in procoagulant-spreading.

In addition, acetazolamide and hyperosmotic challenge significantly reduced PS exposure and thrombin generation on the platelet surface (**Figures 7C&D, S3B** and **Movies S9, 10**). The mean intensity of thrombin substrate per unit membrane area was similar in BAPS and BNS platelets (**Figure 7E**), suggesting that the greater thrombin generation seen in controls was due to increased membrane surface area provided by ballooning and procoagulant-spreading.

DOI: 10.1161/CIRCULATIONAHA.114.015036

Blocking water entry and ballooning significantly reduces *in vivo* thrombus formation.

Mice were treated by bolus intravenous administration of acetazolamide (7 mg/kg) and carotid artery damage was induced by application of $FeCl_3$ (10% $^{v}/_{v}$). Accumulation of platelets, labelled with DyLight 488-antiGp1bα, was visualised by video epifluorescence microscopy. Whereas control mice showed rapid and sustained accumulation of platelets in a growing and eventually occlusive thrombus, mice treated with acetazolamide were markedly spared from this event (**Figure 8**). Balloon-enhanced local generation of thrombin will therefore likely form a positive feedback system to further activate platelets and promote coagulation.

Discussion

Platelets are the surveillance cells of the vascular system, detecting vessel damage events and acting as the early and rapid response system to address the damage they recognise. They rapidly adhere to sub-endothelial matrix collagen, recruit more platelets to form an aggregate and stabilise the structure by initiating blood coagulation. This procoagulant activity depends on the surface exposure of negatively charged aminophospholipids, particularly phosphatidylserine (PS), which binds the tenase and prothrombinase complexes. The dynamics of platelet membrane transformation therefore underpin the coagulant response. Previous studies have shown that platelets are able to undergo both membrane blebbing and ballooning upon activation[7-11], and that platelet balloon formation is part of the normal hemostatic response. In particular the studies of Wester et al.,[7, 8] used a template bleeding technique to induce acute wounds to human skin, and excised the wounds at various time periods after wounding. Using histological and electron microscopic approaches they showed the existence of platelet balloons within the structure of the associated thrombus. Importantly they showed that fibrin was deposited in the margins between

platelet balloons, suggesting a functional link between balloon formation and coagulation in vivo. Consistent with this, we demonstrated that activated factor V and X are bound to ballooned platelet membranes (**Fig. S2**). We have determined the molecular regulation of these events, and revealed in real time the formation of a novel ballooned and procoagulant-spread (BAPS) platelet phenotype in a process we termed procoagulant-spreading. The balloon and procoagulant-spread structures are functionally linked and both contribute to the local generation of thrombin. BAPS platelets break into a multitude of procoagulant microvesicles, and this process may form a major route for generation of platelet-derived microvesicles which contribute to local hemostasis but with potential for pathological roles in various cardiovascular diseases[25].

While previous studies had described platelet membrane ballooning in some detail[7, 8, 10, 11, 26], this is the first report of coordinated membrane ballooning and procoagulant-spreading. Platelets with characteristics similar to the ballooned platelets seen here have been reported, particularly COATED and SCIP platelets[18, 26]. However, there are clear differences, since platelets in this study showed sustained integrin $\alpha_{IIb}\beta_3$ activation (**Figures 1G,H & S2**) and transient increase in cytosolic calcium (data not shown). Furthermore, data in **Figure S2 and S4b** show that the balloon retains some of the molecular and subcellular components of the platelet from which it was derived, including various surface receptor markers and mitochondria.

The timing and localisation of PS exposure in platelets indicates that it does not appear until ballooning is well under way, suggesting that PS exposure is not a requirement for ballooning. Rather, platelet balloons result from physical disruption to the circumferential microtubule, accompanied by an increase in internal hydrostatic pressure provided by a coordinated Na^+, Cl^- and water entry mechanism, which inflates the balloon. By contrast, membrane blebbing analogous to that seen in cancerous cells is reversible and occurs

independent of fluid entry mechanisms[27]. It is possible that Na^+ may enter through non-selective cation channels, such as TRPC6[28], or by Na^+/Ca^{2+} exchange. For Cl^-, anoctamin (TMEM16) genes are key components of calcium-activated chloride channels, (CaCC)[29-31]. Anoctamin-6 is a CaCC[6, 32] which functionally couples to TRPC channels[33]. Salt may therefore enter through regulated pathways, providing an osmotic drive for water entry and ballooning. The role of calcium in these events is pivotal since blockade of calcium entry or release from intracellular stores abolished ballooning and procoagulant-spreading, but not lamellipodial spreading (data not shown). A rise in cytosolic free Ca^{2+} may therefore trigger CaCC opening[6] and allow chloride entry[34]. Interestingly, the rise in cytosolic Na^+ and Cl^- ions concentrations are predominantly in the platelet cell body, rather than the balloon (**Figure 6**). A possible explanation is that the major volume change occurs in the balloon, and not in the cell body. Likely, all increases in ion concentration in the balloon are continuously being diluted through entry of water. Related to this, we have never observed balloons to continue to grow or to burst, but always observe them reaching a plateau size. We suggest that this is likely to be a product of this transient increase in ion permeability leading to a self-limiting water entry, constraining the balloon to a steady-state sustained volume.

Scott syndrome is extremely rare and patients show a bleeding disorder associated with defective expression of TMEM16F and a resultant defect in microvesicle formation and exposure of PS[5, 35]. Our observations show that platelet ballooning is also markedly impaired in this syndrome (**Figure 1C**). It is possible that TMEM16F provides the critical mechanism driving ballooning, through regulated ion influx followed by water, and that the membrane stretching lowers the activation energy required for scrambling of membrane phospholipids and movement of inner leaflet PS to the outer leaflet.

Importantly, this study has revealed a novel phenotype which we have termed ballooned and procoagulant-spread (BAPS) platelets. These structures break up to form procoagulant microvesicles and thereby increase the PS-exposing membrane surface area for procoagulant activity. That it had been previously missed in the literature was likely the result of the extremely thin and particulate nature of the spread membrane, which is only visible when platelets are stained with labelled annexin-V, under physiological concentrations of extracellular calcium and monitored over varying z-heights. There was a direct link between ballooning and procoagulant-spreading because inhibition of ballooning by CaCCinh-A01 (**Figure 6E**) or jasplakinolide or acetazolamide (**Figures 5 & 7**) also blocked procoagulant-spreading and microparticle generation (**Figure S3**). Agents that inhibit procoagulant-spreading independent of ballooning, such as blebbistatin, cytochalasin-D or Y27632, also largely inhibited microparticle formation (**Figure S3**). It is therefore likely that all these events are functionally linked, and sequential, from ballooning to procoagulant-spreading to microparticle formation (**Movies S5&S6**). It is interesting to note that endothelial PS exposure has recently been shown to play a major role in thrombin generation[36]. However, it is possible that procoagulant-spreading may also allow platelets to contribute to coagulation over a much wider surface area than just the platelet 'cell body', which may explain any apparent discrepancy with Ivanciu *et al.* (2014).

Our data would also suggest that as the hydrostatic pressure in the platelet cell body rises, it is able to sustain this increase in pressure due to the intact cytoskeleton of the cell. However, once a weakness in the cytoskeleton develops, the membrane rapidly inflates to generate the balloon. This leaves further questions, such as the molecular nature of the ion and water channels, and whether disruption of the cytoskeleton is a tightly coordinated event. The fact however that acetazolamide is able to markedly diminish *in vitro* ballooning, and also act to

potently inhibit thrombus formation *in vivo*, indicates the importance of this event, and suggests potentially novel ways to control thrombus formation pharmacologically.

In conclusion, this study has uncovered the molecular mechanisms that control dramatic platelet membrane ballooning and revealed a novel procoagulant-spread membrane structure, upon platelet activation by collagen. The events are mechanistically coupled and are likely to amplify the procoagulant responses at wound sites. They also suggest a route by which platelets generate microparticles upon contact with collagen. The mechanism of membrane ballooning shown here, which involves salt and water entry into the cells, may lead to new therapeutic directions for the control of thrombus formation *in vivo*.

Acknowledgments: We acknowledge the MRC and the Wolfson Foundation for funding the University of Bristol's Bioimaging Facility. We thank Alan Leard, Katy Jepson and Judith Mantell of the Wolfson Bioimaging Facility for their assistance. We thank Dr Nicholas Timpson (School of Social and Community Medicine) and Dr Peter Brennan (School of Physiology and Pharmacology) of the University of Bristol, for their help with the statistical review.

Funding Sources: This work was supported by the British Heart Foundation (RG/10/006/28299; PG/12/25/29488; FS/11/62/28934; PG/10/100/28658; FS/12/22/29510), Netherlands Heart Foundation (2011T6 to JMEMC), ZonMW (MKMD 114021004 to JMEMC and JWMH), and United Kingdom National Institute for Health Research (II-LB-0313-20003).

Conflict of Interest Disclosures: None.

References:

1. Jackson SP. Arterial thrombosis - insidious, unpredictable and deadly. *Nat Med*. 2011;17:1423-1436.

2. Suzuki J, Umeda M, Sims PJ, Nagata S. Calcium-dependent phospholipid scrambling by TMEM16F. *Nature*. 2010;468:834-838.

3. Kunzelmann K, Nilius B, Owsianik G, Schreiber R, Ousingsawat J, Sirianant L, Wanitchakool P, Bevers E, Heemskerk JM. Molecular functions of anoctamin 6 (TMEM16F): a chloride channel, cation channel, or phospholipid scramblase? *Pflugers Arch - Eur J Physiol*. 2014;466:407-414.

4. Castoldi E, Collins PW, Williamson PL, Bevers EM. Compound heterozygosity for 2 novel TMEM16F mutations in a patient with Scott syndrome. *Blood*. 2011;117:4399-4400.

5. Zwaal RFA, Comfurius P, Bevers EM. Scott syndrome, a bleeding disorder caused by defective scrambling of membrane phospholipids. *Biochim Biophys Acta*. 2004;1636:119-128.

6. Tian Y, Schreiber R, Kunzelmann K. Anoctamins are a family of Ca2+-activated Cl− channels. *J Cell Sci.* 2012;125:4991-4998.

7. Wester J, Sixma J, Geuze J, Heijnen H. Morphology of the hemostatic plug in human skin wounds: transformation of the plug. *Lab Invest.* 1979;41:182-192.

8. Wester J, Sixma J, Geuze J, van der Veen J. Morphology of the early hemostasis in human skin wounds: influence of acetylsalicylic acid. *Lab Invest.* 1978;39:298-311.

9. Sixma JJ, Van Den Berg A. The haemostatic plug in haemophilia A: a morphological study of haemostatic plug formation in bleeding time skin wounds of patients with severe haemophilia A. *Br J Haematol.* 1984;58:741-753.

10. Heemskerk JWM, Vuist WMJ, Feijge MAH, Reutelingsperger CPM, Lindhout T. Collagen But Not Fibrinogen Surfaces Induce Bleb Formation, Exposure of Phosphatidylserine, and Procoagulant Activity of Adherent Platelets: Evidence for Regulation by Protein Tyrosine Kinase-Dependent Ca2+ Responses. *Blood*. 1997;90:2615-2625.

11. Hess MW, Siljander P. Procoagulant platelet balloons: evidence from cryopreparation and electron microscopy. *Histochem Cell Biol.* 2001;115:439-443.

12. Heemskerk JWM, Siljander P, Vuist WMJ, Breikers G, Reutelingsperger CPM, Barnes MJ, Graham Knight C, Lassila R, Farndale RW. Function of Glycoprotein VI and Integrin a2b1 in the Procoagulant Response of Single, Collagen-Adherent Platelets. *Thromb Haemost*. 1999;81:782-792.

13. Rudolf E, Peychl J, Novak J, Cervinka M. Apoptosis - when the cells begin to dance. *Front Biosci.* 2000 5:1-2.

14. Sebbagh M, Renvoize C, Hamelin J, Riche N, Bertoglio J, Breard J. Caspase-3-mediated cleavage of ROCK I induces MLC phosphorylation and apoptotic membrane blebbing. *Nat Cell Biol*. 2001;3:346-352.

15. Coleman ML, Sahai EA, Yeo M, Bosch M, Dewar A, Olson MF. Membrane blebbing during apoptosis results from caspase-mediated activation of ROCK I. *Nat Cell Biol*. 2001;3:339-345.

16. Jackson SP, Schoenwaelder SM. Procoagulant platelets: are they necrotic? *Blood*. 2010;116:2011-2018.

17. Abaeva AA, Canault M, Kotova YN, Obydennyy SI, Yakimenko AO, Podoplelova NA, Kolyadko VN, Chambost H, Mazurov AV, Ataullakhanov FI, Nurden AT, Alessi M-C and Panteleev MA. Procoagulant Platelets Form an α-Granule Protein-covered "Cap" on Their Surface That Promotes Their Attachment to Aggregates. *J Biol Chem*. 2013;288:29621-29632.

18. van Kruchten R, Mattheij NJA, Saunders C, Feijge MAH, Swieringa F, Wolfs JLN, Collins PW, Heemskerk JWM and Bevers EM. Both TMEM16F-dependent and TMEM16F-independent pathways contribute to phosphatidylserine exposure in platelet apoptosis and platelet activation. *Blood*. 2013;121:1850-1857.

19. López JA, Andrews RK, Afshar-Kharghan V, Berndt MC. Bernard-Soulier Syndrome. *Blood*. 1998;91:4397-4418.

20. van de Vijver E, De Cuyper IM, Gerrits AJ, Verhoeven AJ, Seeger K, Gutiérrez L, van den Berg TK, Kuijpers TW. Defects in Glanzmann thrombasthenia and LAD-III (LAD-1/v) syndrome: the role of integrin β1 and β3 in platelet adhesion to collagen. *Blood*. 2012;119:583-586.

21. Michelson AD. Gray platelet syndrome. *Blood*. 2013;121:250-250.

22. Kovács M, Tóth J, Hetényi C, Málnási-Csizmadia A, Sellers JR. Mechanism of Blebbistatin Inhibition of Myosin II. *J Biol Chem*. 2004;279:35557-35563.

23. Holzinger A. Jasplakinolide: An Actin-Specific Reagent that Promotes Actin Polymerization. In: R. H. Gavin, ed. *Cytoskeleton Methods and Protocols*: Humana Press; 2010(586): 71-87.

24. Gao J, Wang X, Chang Y, Zhang J, Song Q, Yu H, Li X. Acetazolamide inhibits osmotic water permeability by interaction with aquaporin-1. *Anal Biochem*. 2006;350:165-170.

25. Italiano JJ, Mairuhu A, Flaumenhaft R. Clinical relevance of microparticles from platelets and megakaryocytes. *Curr Opin Hematol*. 2010;17 578-584.

26. Kulkarni S, Jackson SP. Platelet Factor XIII and Calpain Negatively Regulate Integrin αIIbβ3 Adhesive Function and Thrombus Growth. *J Biol Chem*. 2004;279:30697-30706.

27. Fackler OT, Grosse R. Cell motility through plasma membrane blebbing. *J Cell Biol*. 2008;181:879-884.

28. Harper MT, Londono JEC, Quick K, Londono JC, Flockerzi V, Philipp SE, Birnbaumer L, Freichel M and Poole AW. Transient Receptor Potential Channels Function as a Coincidence Signal Detector Mediating Phosphatidylserine Exposure. *Sci Signal.* 2013;6:ra50 (1-11).

29. Yang YD, Cho H, Koo JY, Tak MH, Cho Y, Shim W-S, Park SP, Lee J, Lee B, Kim B-M,

Raouf R, Shin YK, Oh U. TMEM16A confers receptor-activated calcium-dependent chloride conductance. *Nature*. 2008;455:1210-1215.

30. Schroeder BC, Cheng T, Jan YN, Jan LY. Expression Cloning of TMEM16A as a Calcium-Activated Chloride Channel Subunit. *Cell*. 2008;134:1019-1029.

31. Caputo A, Caci E, Ferrera L, Pedemonte N, Barsanti C, Sondo E, Pfeffer U, Ravazzolo R, Zegarra-Moran O, Galietta LJV. TMEM16A, A Membrane Protein Associated with Calcium-Dependent Chloride Channel Activity. *Science*. 2008;322:590-594.

32. Grubb Sr, Poulsen KA, Juul CAl, Kyed T, Klausen TK, Larsen EH, Hoffmann EK. TMEM16F (Anoctamin 6), an anion channel of delayed Ca2+ activation. *J Gen Physiol*. 2013;141:585-600.

33. Viitanen TM, Sukumaran P, Löf C, Törnquist K. Functional coupling of TRPC2 cation channels and the calcium-activated anion channels in rat thyroid cells: Implications for iodide homeostasis. *J Cell Physiol*. 2013;228:814-823.

34. Paradiso AM, Ribeiro CMP, Boucher RC. Polarized Signaling via Purinoceptors in Normal and Cystic Fibrosis Airway Epithelia. *J Gen Physiol*. 2001;117:53-68.

35. Munnix ICA, Harmsma M, Giddings JC, Collins PW, Feijge MAH, Comfurius P, Heemskerk JWM, Bevers EM. Store-mediated calcium entry in the regulation of phosphatidylserine exposure in blood cells from Scott patients. *Thromb Haemost*. 2003;89:687-695.

36. Ivanciu L, Krishnaswamy S, Camire RM. New insights into the spatiotemporal localization of prothrombinase in vivo. *Blood*. 2014;124:1705-1714.

Figure Legends:

Figure 1. Spatiotemporal dynamics of human platelets undergoing ballooning and a procoagulant response upon adhesion to collagen. (**A**) & (**B**) Platelets were allowed to adhere to a collagen-coated surface and imaged by phase contrast video microscopy. Images show the time course of interaction of a single platelet, with frame numbers in (**A**) corresponding to the time points shown in (**B**). Three distinct phases of ballooning are shown as Ph_1, Ph_2 and Ph_3. See also Movie S1. (**C**) Rotated views of a 3D reconstruction of Alexa568-Annexin-V (AnxV; red)

stained ballooned platelet in Ph_3. See also Movie S2. (**D-F**) Time course of a platelet undergoing ballooning upon adhesion to a collagen-coated surface. Alexa568-AnxV-stained fluorescence images in (upper panel **D**, see also Movie S3) are superimposed upon phase contrast images (lower panel **D**). Image frame numbers correspond to time points indicated in (**E**) & (**F**). (**E**) displays the time course of AnxV staining in the platelet cell body and balloon, and the early time course after adhesion to collagen is indicated in the inset (**F**). (**G**) Extended focus image showing Oregon green-488 human fibrinogen staining for activated integrin $\alpha_{IIb}\beta_3$ (green) and Alexa568-AnxV (red). The time course for fibrinogen (green) and AnxV (red) binding is shown in (**H**). Scale bars: (**A**, **C**, **D**, **G**) 2μm, (**B, E** & **F**) 5 min. Data are representative of 257 platelets from 9 donors.

Figure 2. Thrombin is generated on the ballooned surface of human platelets adherent to collagen: Scott patient platelets show aberrant membrane ballooning. (**A**) Platelets in platelet-rich plasma were allowed to settle onto a collagen-coated surface, and thrombin activity was visualized in real-time, by means of a fluorogenic thrombin substrate, Z-GGR-AMC. **A(i)** Z-section of confocal image at 15 min shows the fluorogenic thrombin substrate on the membranes of ballooned platelets. **A(ii)** 3D reconstruction of platelets in A(i). **A(iii)** shows the first derivative of the time course of thrombin generation in a representative single platelet after adhesion to the collagen-coated surface. Scale bars in (**i**) and (**ii**) are 3 μm. . (**B**) Blood from healthy control (**i**) or a patient with Scott syndrome (**ii**) was flowed over a collagen-coated surface at 1000 s^{-1} for 4 min. Accumulated thrombi were stained with FITC-αCD62P mAb to detect P-selectin. Arrows indicate platelet balloons. Scale bars in (**i**) and (**ii**) are 5 μm. Data are representative of platelets from at least 3 donors (healthy) except Scott patient data in **B(ii)** where n=1.

Figure 3. A distinct subpopulation of ballooning platelets undergo extensive procoagulant-spreading. Platelets were allowed to adhere to a collagen-coated surface for 1 hour and imaged by phase contrast and fluorescence video microscopy. (**A**) shows an overlay of phase contrast with Alexa568-Annexin-V (AnxV; red) and Fluo-4 (green). Four phenotypes were observed, as indicated: non-ballooned non-spread platelets (NBNS), ballooned non-spread platelet (BNS), conventional spread non-ballooned platelet (CSNB) and ballooned and procoagulant-spread platelet (BAPS). (**B**) Z sections of the image shown in (A) at the indicated distance above the coated surface. Shown are phase-contrast (i), Alexa568-AnxV (red, ii), Alexa568-AnxV (red) superimposed on Fluo-4 (green, iii), and combined overlay (iv). Scale bar: 10 μm. Data are representative of platelets from 9 human donors. See also associated Movie S4.

Figure 4. Membrane ballooning and procoagulant-spreading are coordinated events. **(A-C)** Platelets were allowed to adhere to a collagen-coated surface and imaged by 4D fluorescence microscopy. A time series of 3D reconstructions of a ballooned and procoagulant-spread (BAPS) platelet is shown in the X-Y axis (A, and see Movie S5) and X-Y-Z axis (B, and see Movie S6). Images are superimposed Alexa568-Annexin-V (AnxV; red) and $DiOC_6$ (green). Spread membrane and balloon diameter of this platelet are shown in **C(i)**, while **C(ii)** indicates the percentage of adherent platelets showing different phenotypes after 1 hr on collagen, abbreviated as per legend for Fig. 3. Data show min to max values, median and interquartile ranges. (**D-F**) Scanning electron microscopy images of platelets adherent to collagen show BAPS and conventional spread non-ballooned (CSNB) phenotypes as indicated (**F** is a zoomed-in view of inset in **E**). Scale bar: 12 μm (**A, B**), 3 μm (**D-F**). Data are representative of platelets from 9 human donors.

Figure 5. Inhibition of actomyosin contraction promotes membrane ballooning whilst blocking procoagulant-spreading. Platelets were pre-incubated with DMSO (0.1%; control), blebbistatin (BBS; 80 µmol/L), cytochalasin-D (Cyt-D; 5 µmol/L), Y27632 (10 µmol/L) or jasplakinolide (Jaspl; 5 µmol/L) and allowed for 1 h to adhere to collagen coated surface. (**A**) (i) Top row shows extended focus fluorescence images of Alexa568-Annexin-V (AnxV; red), which were overlaid with phase-contrast images in bottom row. (ii) Interleaved box plots with whiskers showing min to max values, median and interquartile range. Graph indicates the percentage of adherent platelets observed showing different phenotypes. For abbreviations, see text for Fig. 3. Data analysis was by Friedman test, followed by Dunn's multiple comparison test. $P < 0.05$ (*) or $P < 0.01$ (**) was considered significant. (**B**) Mean intensity per platelet versus time plot, of the fluorogenic thrombin substrate, after adhesion to collagen. Extended focus fluorescence images are control (i, ii) or cyto-D treated platelets (iii, iv) detecting thrombin substrate alone (cyan blue, i & iii) or overlaid with AnxV (ii & iv). (**C**) 3D reconstruction of adherent platelets stained with (i) fluo-4 (green), (ii) AnxV (red) and (iii) phalloidin (magenta), distinguishing CSNB and BAPS phenotypes as indicated. White and yellow bracket in C(ii) delineate the ballooned and procoagulant-spread segments of the BAPS platelet. C-iv shows an overlay of i - iii. Scale bar: 12 µm (**A, B**), 10 µm (**C**). Data are representative of platelets from 6 human donors. See also Movie S7 and Figure S3.

Figure 6. Membrane ballooning and procoagulant-spreading is mediated by salt entry. **(A-D)** Platelets were pre-loaded with the chloride ion (Cl^-) indicator MQAE (**A,B**) or the sodium ion (Na^+) indicator CoroNa™ Green (**C,D**). Cells were allowed to adhere to immobilised collagen and time-lapse fluorescence images captured. Images show the time course of interaction of a single platelet, with frame numbers in (**A**) & (**C**) corresponding to the time points shown in (**B**)

& (**D**) respectively. Images in (**A**) show MQAE alone (Cyan blue, i), overlaid onto phase-contrast image (ii) or on to Alexa568-Annexin-V (AnxV; red, iii). (**B**) shows fluorescence quantification (F/F_0) for MQAE and Alexa568-AnxV, and mean balloon diameter. MQAE detects chloride ion entry by collisional quenching, thus decreases in F/F_0 against time represent increases in $[Cl^-]_i$. Images in (**C**) show CoroNa™ Green alone (green, i) or overlaid on to phase-contrast image (ii). (**D**) shows fluorescence quantification (F/F_0) for CoroNa™Green and mean balloon diameter. (**E&F**) Platelets were pre-treated with DMSO (0.1%; control) or CaCCinh-A01 (40 μmol/L) or resuspended in Cl^--free or Na^+-free media, and added to collagen-coated surfaces. The percentage of maximally adherent platelets undergoing membrane blebbing or ballooning over time is shown in (**E**). Corresponding images are shown in the lower panels where AnxV (red) images are superimposed onto phase-contrast images. (**F**) shows phenotypes (abbreviated as per Fig. 3) of platelet adherent to collagen at 1 h time point; in interleaved box plots with whiskers showing min to max values, median and interquartile range. Data analysis was by Friedman test, followed by Dunn's multiple comparison test. $P < 0.05$ (*) or $P < 0.01$ (**) was considered significant. Scale bars: 3 μm (**A, C**), 10 μm (**E**). Time scale (**B**, **D**, **E**): 15 min. Data are representative of platelets from 7 human donors.

Figure 7. Water entry drives platelet membrane ballooning and procoagulant-spreading. (**A**) Platelets were untreated (control), resuspended in hyperosmolar solution (+40 mOsmol) or pre-incubated with acetazolamide (40 μmol/L) and allowed 1 h, to settle onto collagen-coated surface. Graphs show the percentage of maximally adherent platelets undergoing membrane blebbing or ballooning over time. Lower panels show representative images of Alexa568-Annexin-V (AnxV) stained platelets (red) superimposed on corresponding phase-contrast images. (**B**) Bar chart shows the percentage of adherent platelets observed showing different

phenotypes, abbreviated as per Fig. 3; in interleaved box plots with whiskers showing min to max values, median and interquartile range. Data analysis was by Friedman test, followed by Dunn's multiple comparison test. $P < 0.05$ (*) or $P < 0.01$ (**) was considered significant. (**C**) extended focus fluorescence images showing fluorogenic thrombin substrate (cyan) (i: control, iii: acetazolamide) alone and superimposed onto AnxV stained platelets (red) (ii: control, iv: acetazolamide). (**D**) Fluoresence intensity versus time plot for fluorogenic thrombin substrate. (**E**) Specific fluorescence intensity of the thrombogenic substrate relative to platelet surface area of control and acetazolamide-treated platelets. Scale bar: 15 min (**A**, graphs), 10 μm (**A** lower panels, **C**). Data are representative of platelets from 6 human donors. See also Movie S9 and S10 for videos of acetazolamide-treated and hyperosmolar-treated platelets undergoing reversible ballooning.

Figure 8. Acetazolamide suppresses thrombus formation in vivo. Mice were administered acetazolamide (7mg/kg) or vehicle by single bolus IV injection, followed immediately by DyLight 488-conjugated anti-GPIbβ antibody to label platelets. Carotid artery damage was achieved by treatment with $FeCl_3$ as described in supplementary material. Fluorescently labelled platelets adhering at the site of injury could then be imaged continuously by intravital fluorescence microscopy. Images at frames indicated in (**A**) correspond to time points indicated in (**B (i)**), which shows median fluorescence intensity, quantified using ImageJ. Analysis of area under the curve for media fluorescence is shown in **B (ii)** as interleaved box plots with whiskers showing min to max values, median and interquartile range. Data analysis was by Wilcoxon Signed Rank Test, $P < 0.05$ (*) was considered significant. Scale bar: 500 μM (**A**), 5 min (**B**). Data are from 8 mice.

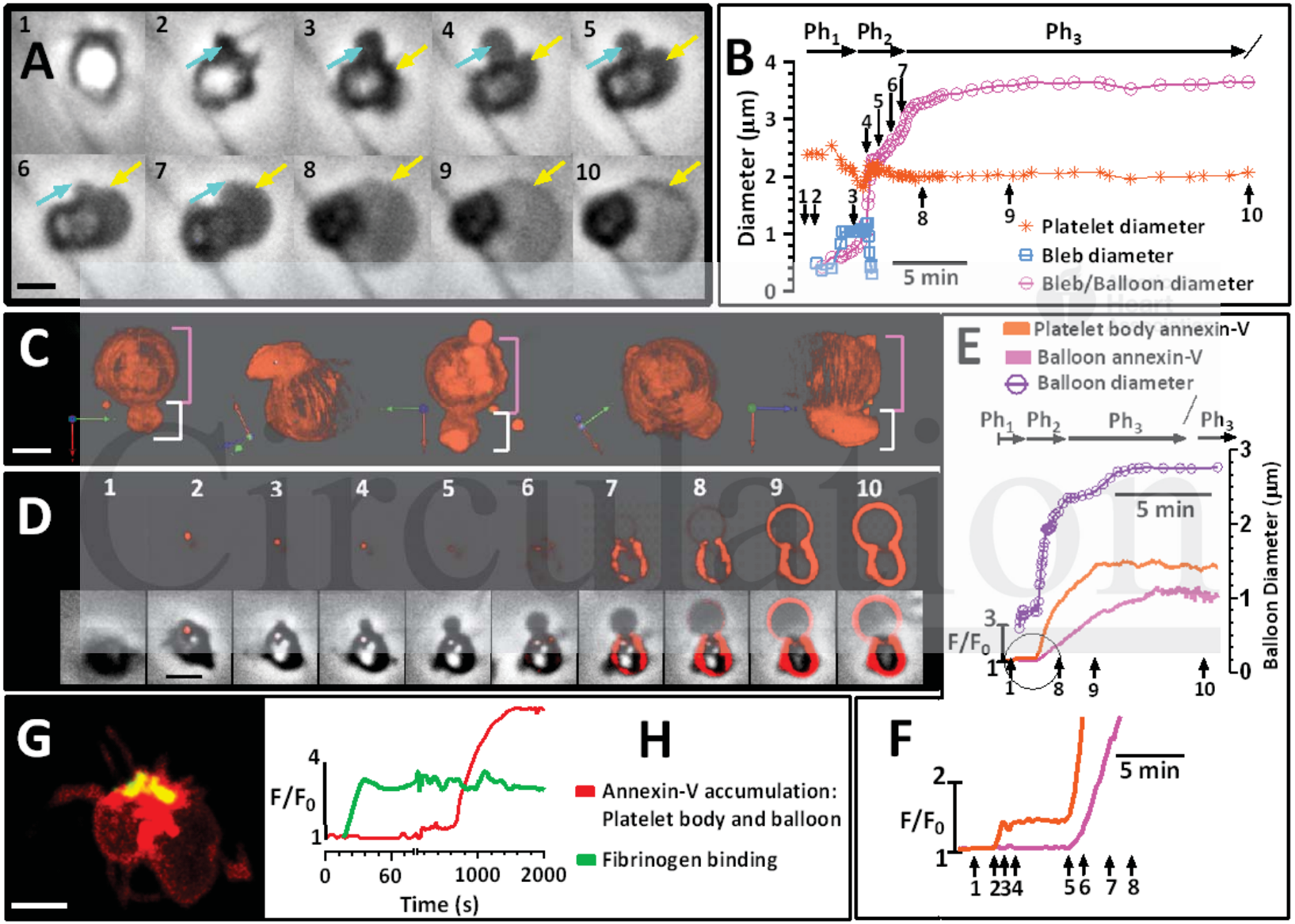

Figure 1

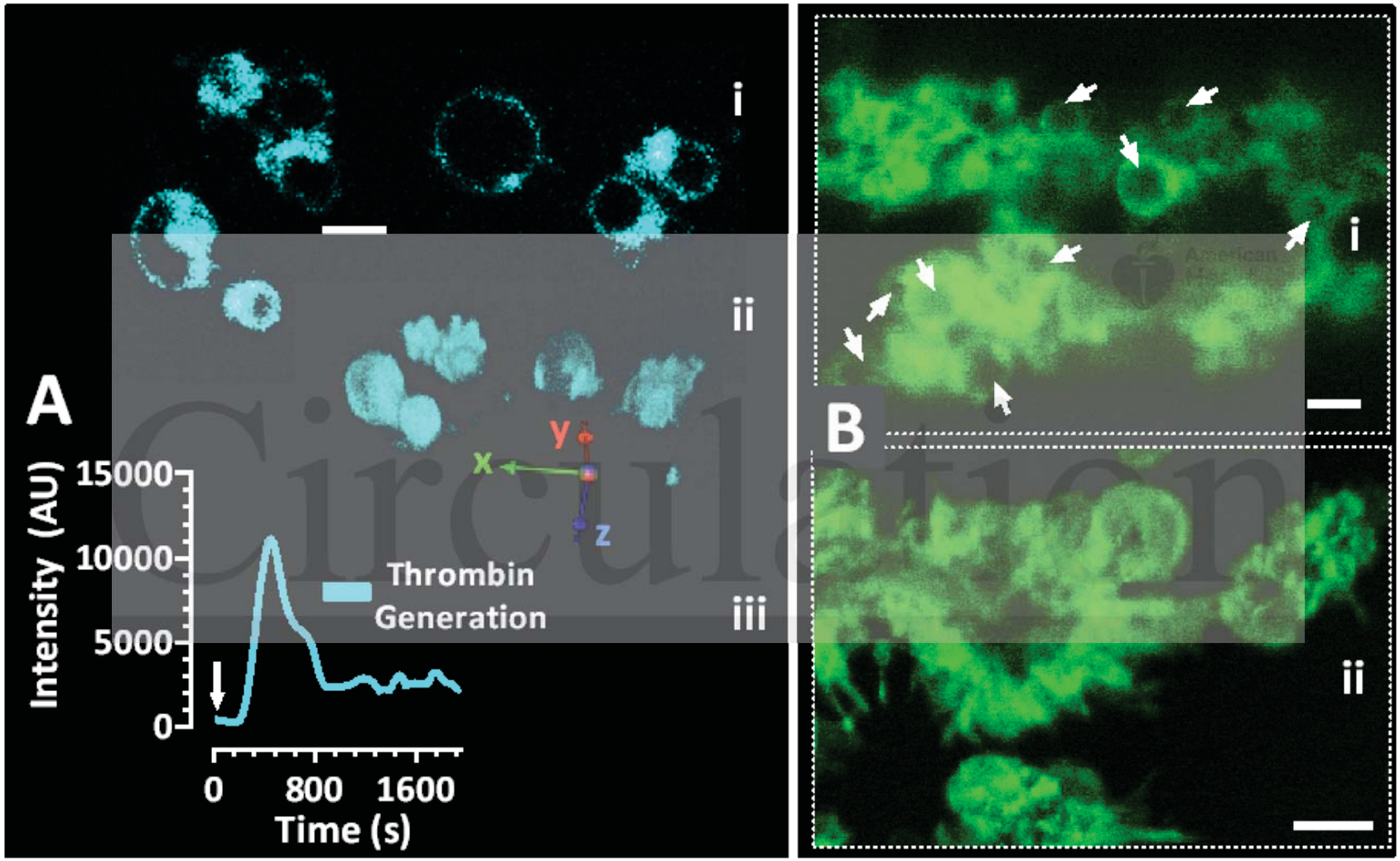

Figure 2

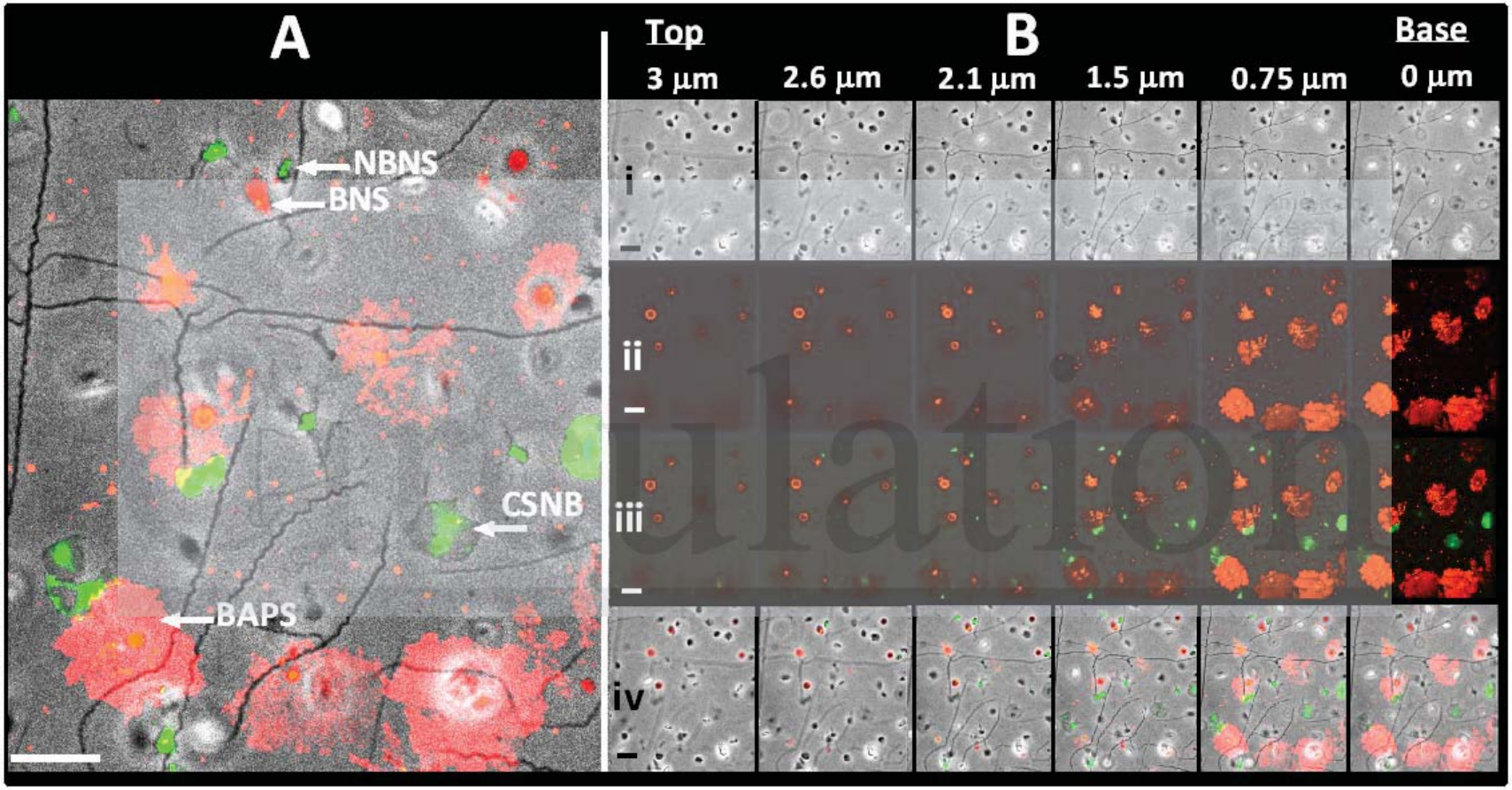

Figure 3

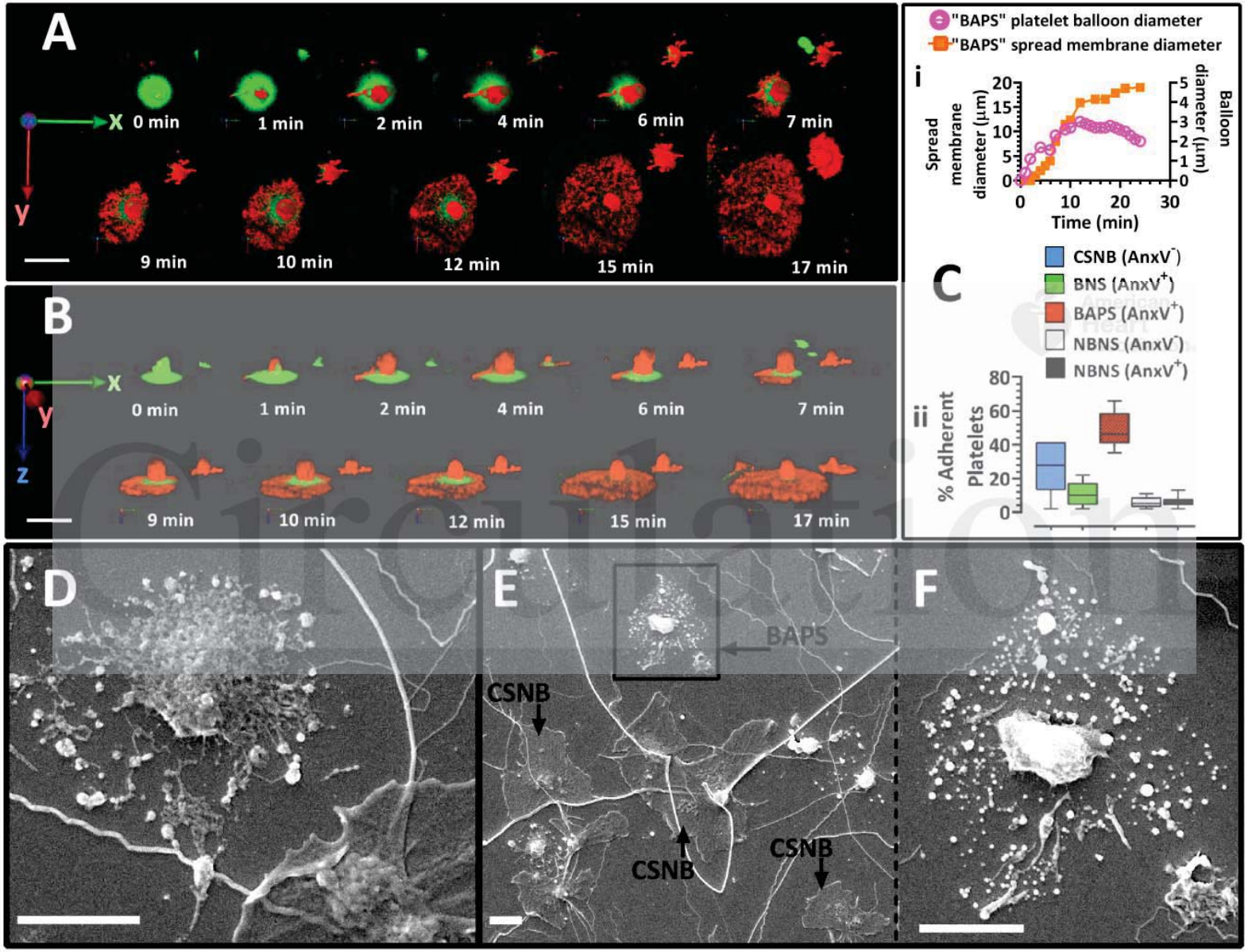

Figure 4

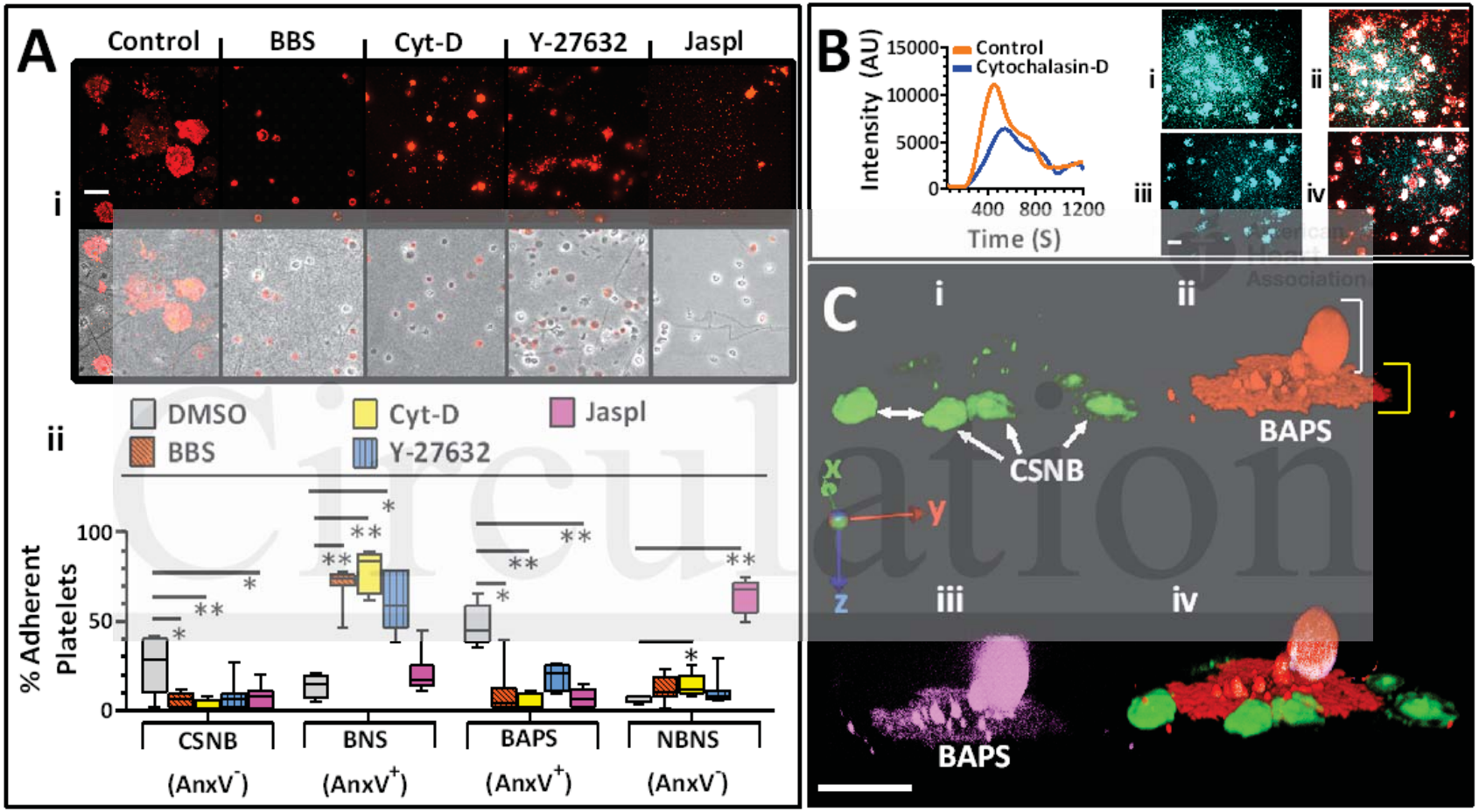

Figure 5

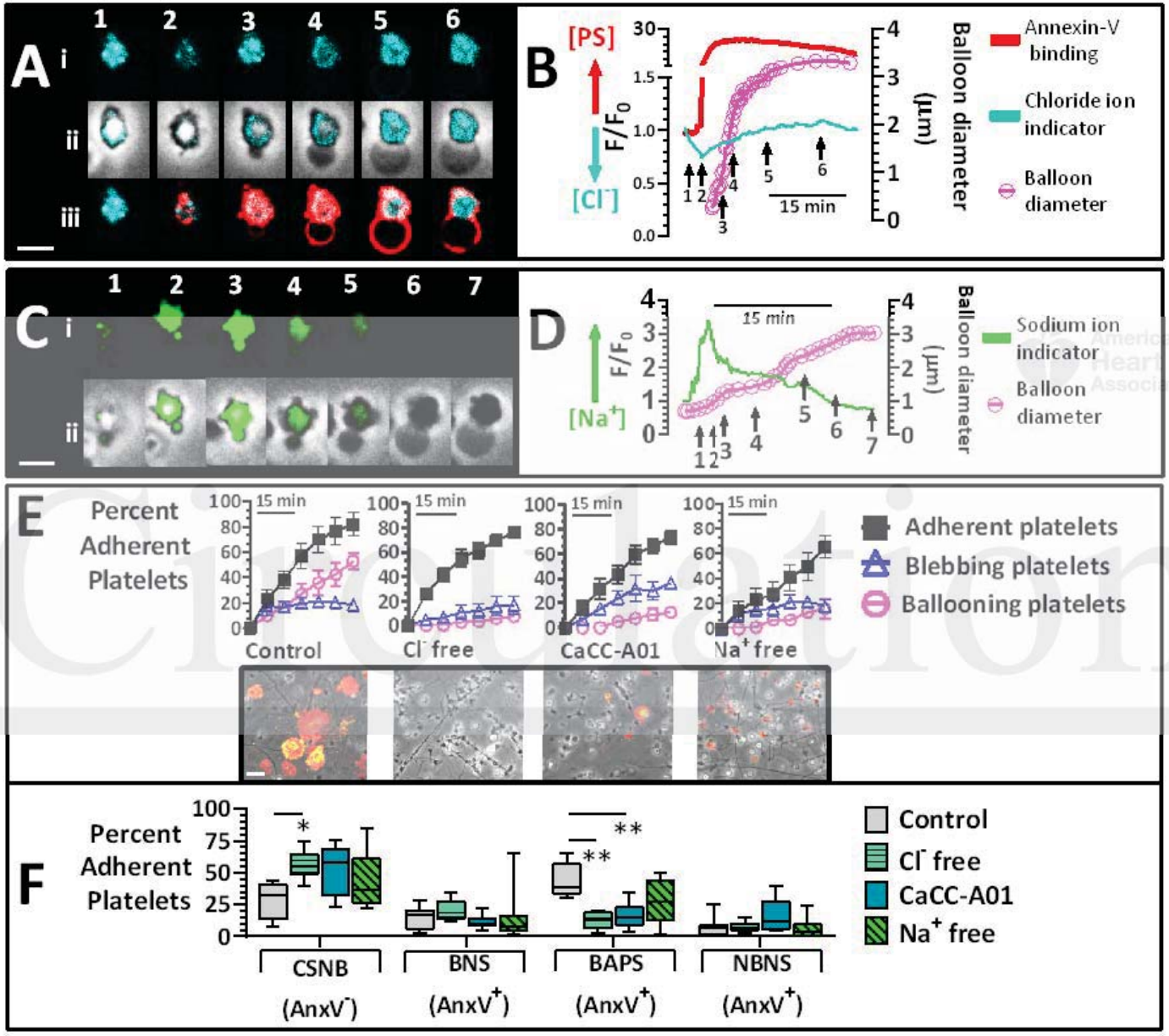

Figure 6

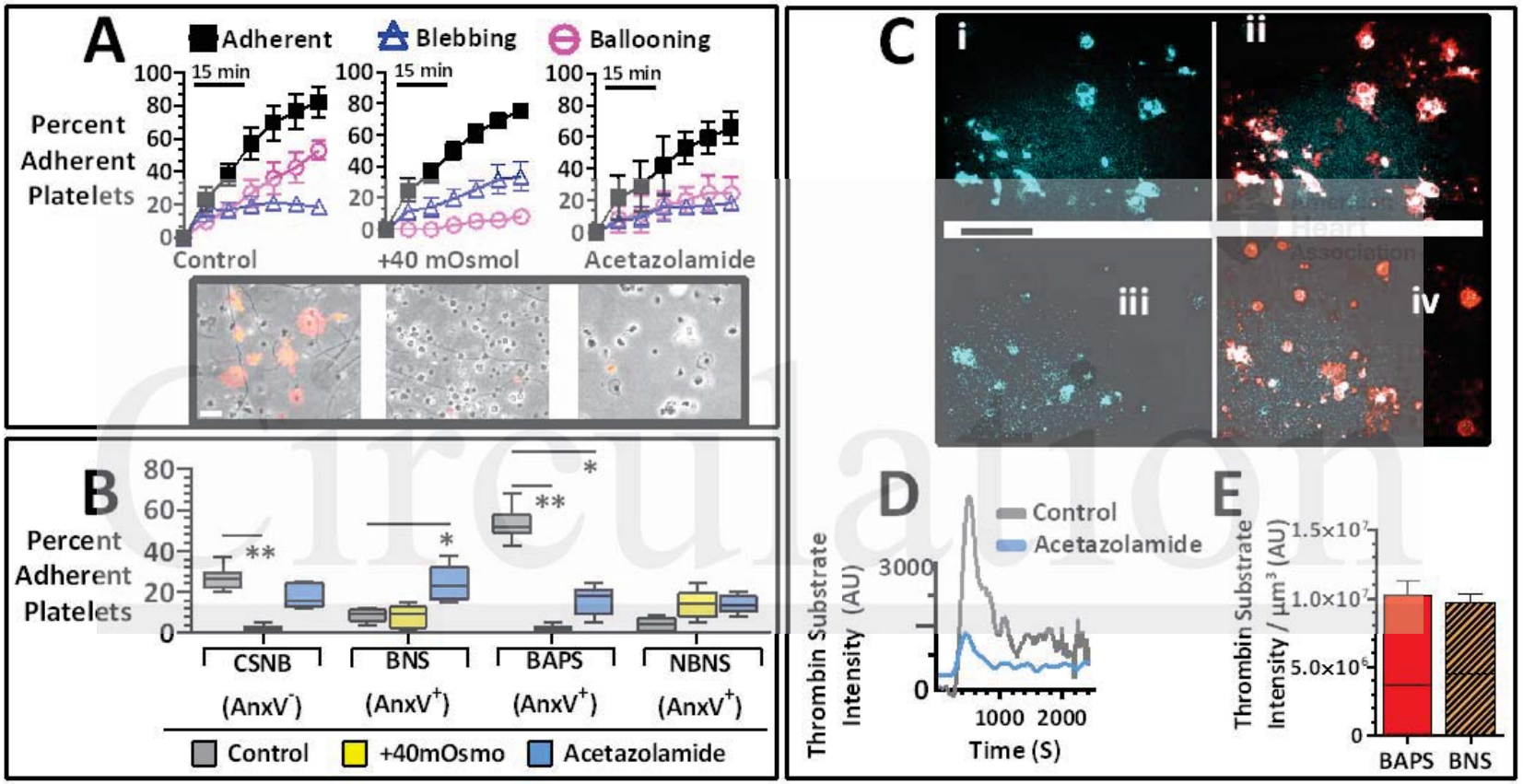

Figure 7

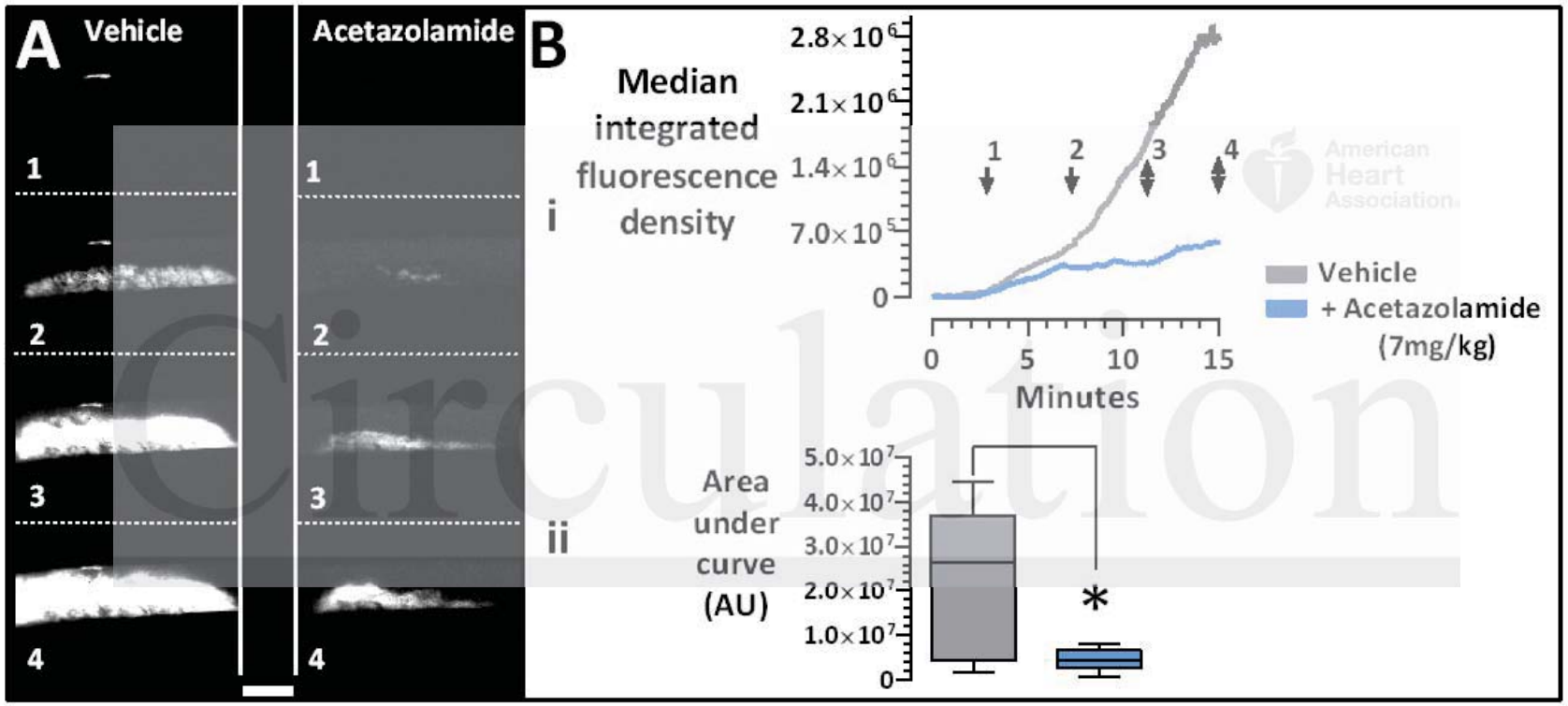

Figure 8

SUPPLEMENTAL MATERIAL

SUPPLEMENTARY METHODS

Materials

Fibrillar collagen (Horm suspension) was from Nycomed (Munich, Germany). Alexa Fluor® 568 Conjugated Annexin V (annexin-V; anxV), Fluo-4 AM, propidium iodide, chloride ion indicator N-(Ethoxycarbonylmethyl)-6-methoxyquinolinium bromide (MQAE), and CoroNa™ green sodium indicator were purchased from Life Technologies. Glass bottom 35mm dishes (P35G-1.5-20-C) were obtained from MatTek Corporation (USA). Flow chambers (Vena8™ biochip) were from Cellix Ltd. BAPTA-AM, blebbistatin, jasplakinolide, cytochalasin-D, Y27632, xestospongin-C and CaCCinh-A01 were purchased from Tocris (Bristol, UK). Acetazolamide was purchased from Sigma-Aldrich (Poole, UK)

Live cell confocal imaging

Confocal images were acquired using a Perkin Elmer Ultra-VIEW ERS 6FE confocal system (with Yokogawa CSU22 spinning disk) attached to a Leica DM I6000 inverted epifluorescence microscope. The system is equipped with Piezo drive, Hamamatsu C9100-50 EM-CCD camera (14 bit, 8 micron pixels) and the following laser lines: 14 mW Ar laser (488, 514 nm lines), 7.5 mW Kr laser (568 nm), 7.5 mW violet (405 nm) diode laser, 7mW blue diode laser (440 nm) and 7.5 mW Red diode (640 nm). Images were captured with Volocity (Improvision) acquisition software using an oil immersion objective lens (100x). Acquisition setting was kept constant and pixel width at x1 binning was 0.069 μm; phase-contrast imaging was integrated with fluorescence imaging using emission discrimination mode. In selected experiments, image acquisition was done in real-time over variable z-heights.

Electron microscopy of mouse carotid artery

The carotid artery was carefully excised and added to 2.5% glutaraldehyde in 0.1 mol/L sodium cacodylate buffer for 1 h. The tissue was post-fixed with 1% osmium tetroxide in sodium cacodylate buffer for 1 h, stained with 3% uranyl acetate in deionised water for 30 min and dehydrated through a graded series of ethanol (70%, 80%, 90%, 96%) followed by three washes in 100% ethanol. The ethanol was replaced with propylene oxide prior to incubation in a 1:1 mixture of propylene oxide and Epon for 24 h. The propylene oxide was left to evaporate for 3 h before the tissue was added to fresh Epon which was hardened for 72 h at 60°C. The artery was sectioned at a thickness of 70 nm.

Correlative light-electron microscopy of platelets

Platelets were seeded into live cell imaging dishes (MatTek) with an etched grid pattern in the glass. Upon completion of fluorescence imaging, the location of the platelets of interest on the grid was noted. Platelets were fixed with 2.5% glutaraldehyde in 0.1mol/L sodium cacodylate buffer (pH7.4) for 30 minutes. Platelets were post-fixed with 1% osmium tetroxide in sodium cacodylate buffer for 30 minutes and stained with 3% uranyl acetate in deionised water for 30 minutes. Platelets were dehydrated through a graded series of ethanol (70%, 80%, 90%, 96%) followed by three washes in 100% ethanol. Platelets were then embedded in pure Epon for 2 hours before being replaced with fresh Epon and hardened for 48 hours at 60°C. The etched coverslip was removed by first submerging in liquid nitrogen and then plunging into boiling water. This process was repeated until the coverslip could be lifted away from the resin. The resin was then trimmed down to the area of interest and sectioned at a thickness of 250 nm. Transmission electron microscopy (TEM) images were

acquired on an Eagle 4k x 4k CCD camera attached to an FEI Tecnai 12, 120kV BioTwin Spirit.

Transmission EM Tomography
Sections were exposed to fiducial markers (10 nm gold particles) on both sides. A dual axis tilt series was acquired using an FEI Tecnai 20, 200kV TEM using a minimum angular range between -60° and +60°, acquiring images at 1° increments. The two tilt series were combined using IMOD reconstruction software.

***In vitro* thrombosis assay**
Flow chambers (Vena8™ biochip) were coated with 50 µg/mL fibrillar collagen for 2 h at 4°C. Chambers were then blocked with 2% fatty acid-free BSA (Sigma Aldrich) overnight at 4°C. Human blood was drawn from healthy volunteers, under local ethics committee agreement and after fully informed consent. Blood was taken into 4% citrate (1:10 v/v) and supplemented with 2 units/mL heparin (Sigma Aldrich) and 40 µmol/L PPACK (Calbiochem). Blood was labelled with 2 µmol/L $DiOC_6$ (3,3′-dihexyloxacarbocyanine iodide) for 10 min in the dark. Immediately prior to being passed through the flow chamber, 6.6 mmol/L $CaCl_2$ and 6.6 mmol/L $MgCl_2$ were added. Blood was passed through the flow chamber at a rate of 1000 s^{-1} for 5 min. The flow chamber was washed for 5 min with HEPES-Tyrode's buffer (10 mmol/L HEPES pH 7.2, 145 mmol/L NaCl, 3 mmol/L KCl, 0.5 mmol/L Na_2HPO_4, 1 mmol/L $MgSO_4$) to remove excess red blood cells. The chamber was visualised by confocal microscopy.

Ferric chloride carotid injury model in mouse
In vivo thrombus formation assays were performed as described here. Mice were bred and experimental procedures performed under UK Home Office licence PPL30/2908, held by AWP. Mice were anaesthetised with ketamine 100 mg/kg (Vetalar V, Pfizer) and 10 mg/kg xylazine (Rompun, Bayer). Acetazolamide or control vehicle was administered by intravenous bolus and platelets were labelled by intravenous administration of 100 mg/kg Dylight-488 conjugated anti-GPIbβ antibody, 10 min prior to induction of thrombosis. Right carotid arteries were exposed and 2x1 mm 15% ferric chloride-soaked filter paper was placed on the arterial adventitia for 3 min. Time-lapse microscopy of the injury site for 20 min was performed and images processed using ImageJ. Background fluorescence values measured upstream of the injury site were subtracted from thrombus-specific fluorescence and data expressed as integrated densities.

SUPPLEMENTARY FIGURES

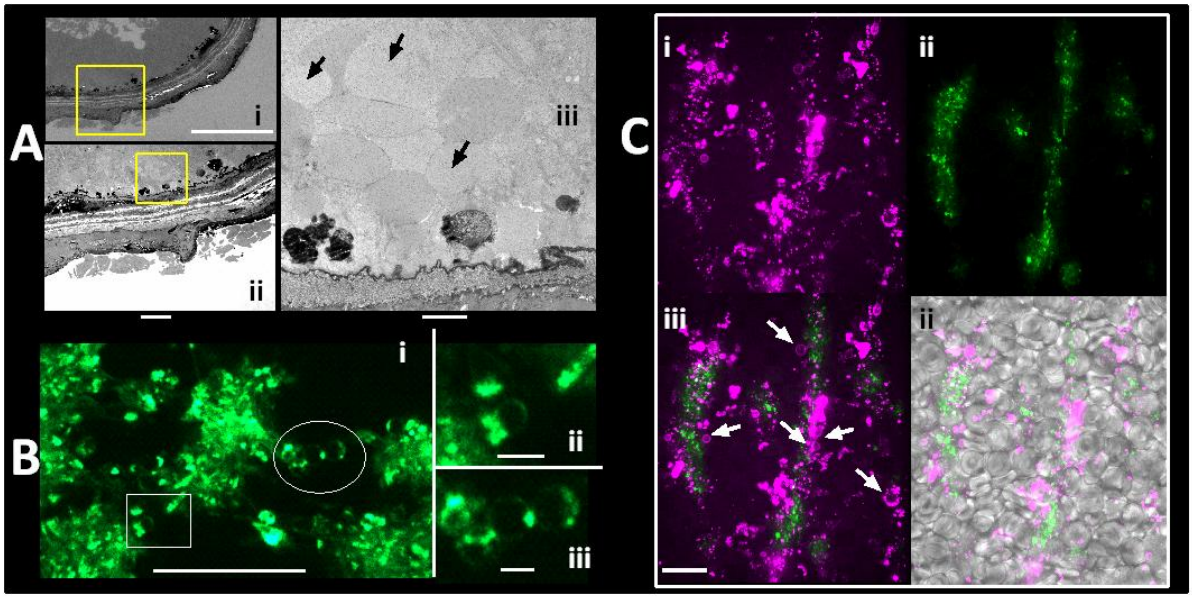

Figure S1: ***In vivo*** **and** ***in vitro*** **evidence for ballooning of human platelet membranes under flow; related to Figure 1.** (A) Electron microscopy of a 30 min biopsy of mouse carotid artery following ferric chloride injury (A-ii and A-iii are zoomed-in views of insets in A-i and A-ii), respectively, with arrows pointing to balloons. (B) Confocal Z-section of a thrombus formed after $DIOC_6$-stained (in green) whole human blood was perfused through collagen-coated capillaries (B-ii and B-iii are zoomed-in views of rectangular and oval insets in B-i, respectively, highlighting ballooned platelets.(C) Extended focus images of thrombus following *in vitro* flow of whole blood over collagen, showing annexin-V-labelled PS (in magenta) (C-i), $DIOC_6$-stained (in green) platelets (C-ii), a combined overlay (C-iii) with arrows showing ballooned platelets, and an overlay onto phase-contrast (C-iv). Scale bar: 50 µm (A-i), 10 µm (A-ii, C), 2 µm (A-iii), 20 µm (B-i), 2 µm (B-ii, B-iii).

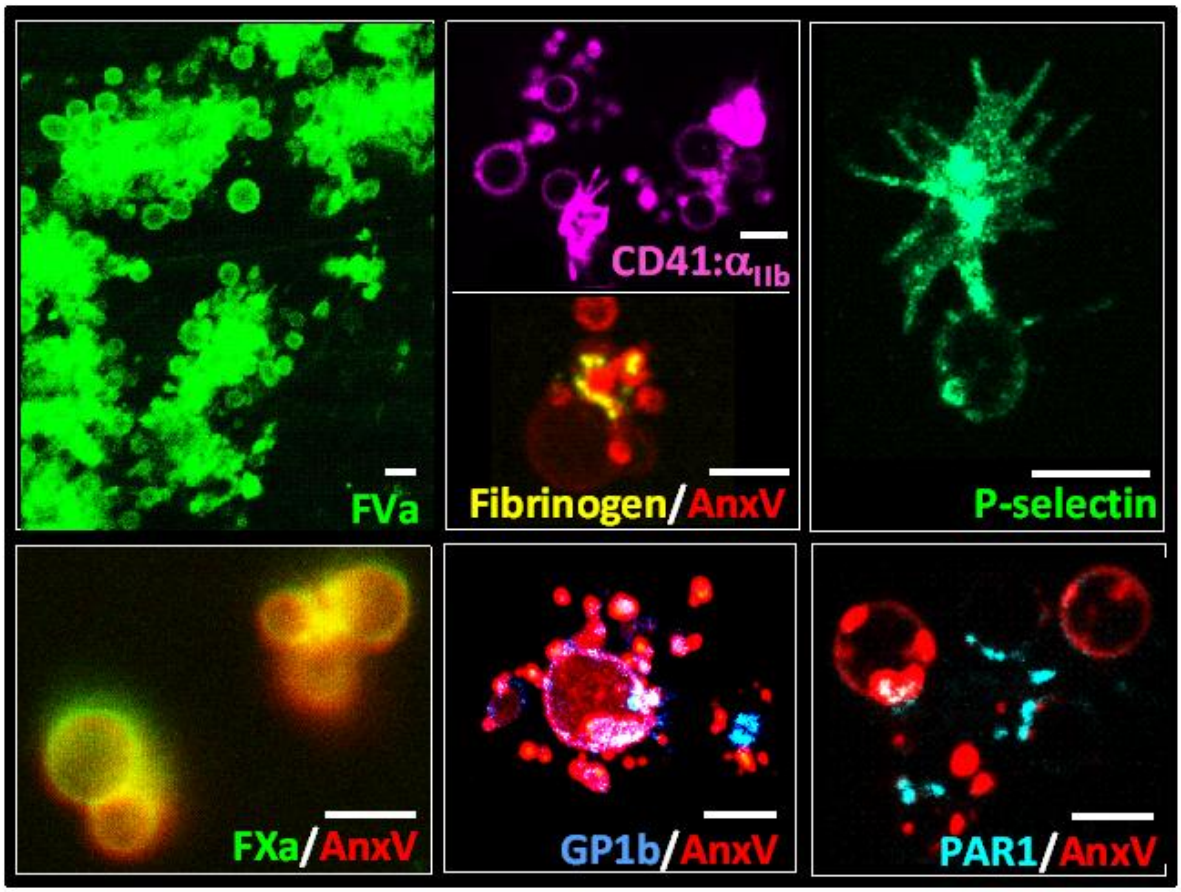

Figure S2: Ballooned human platelets' membrane expressed coagulation markers. Platelets allowed to undergo adhesion and full membrane ballooning (phase 3) over collagen-coated surfaces. Cells were then stained for expression of surface markers with anti FVa, anti FXa, anti-CD41, anti-GP1b, anti-P-selectin and anti-PAR1 and counterstained with Alexa568-AnxV as indicated. Oregon green conjugated human fibrinogen was also used to stain platelets as indicated. Scale bar = 3µm. Data were obtained from platelets analysed from 3 human donors.

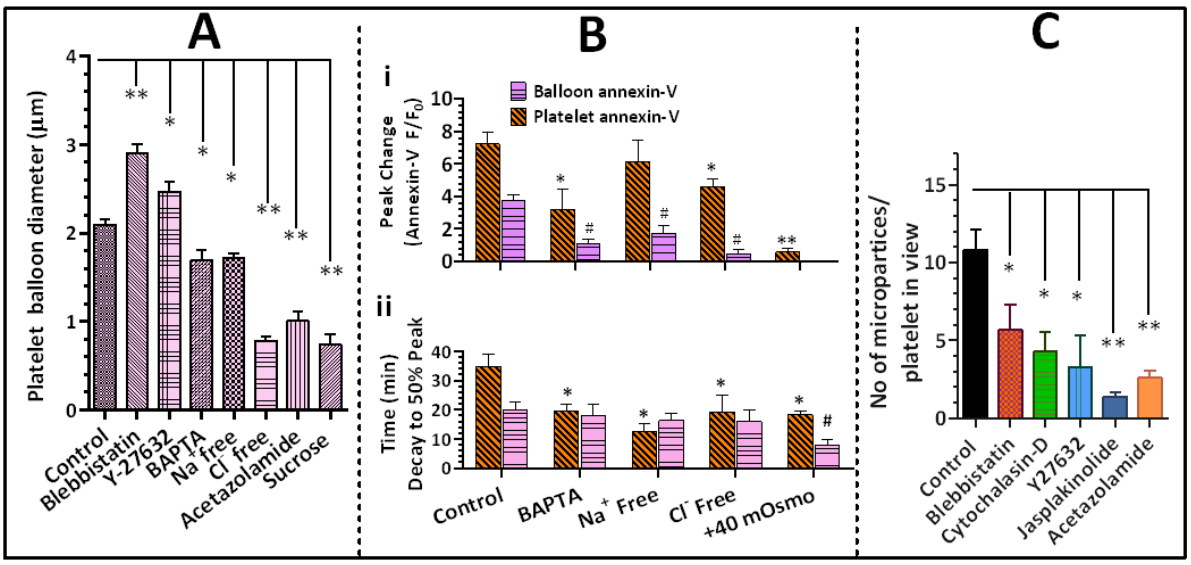

Figure S3: Mean balloon diameter and procoagulant response of human platelet adherent to collagen; related to Figure 2. (A) Platelets, treated as indicated, were monitored as they adhere to collagen. Mean membrane balloon diameter was measured during the stable phase of balloon formation (Ph_3). (B) Spatio-temporal dynamics of phosphatidylserine exposure associated with platelet ballooning as revealed by annexin-V binding to platelets (in orange) or membrane balloons (in magenta). Summary charts show the peak change in annexin-V accumulation (i) and time required for annexin-V intensity to decay to 50% peak values (ii). (C) Microparticles (200-900 nm) released were identified by image intensity and counted; data are expressed as the number of microparticles divided by the number of platelets in the field of view. Data (mean ± SEM) are representative of platelets from 6-9 human donors.

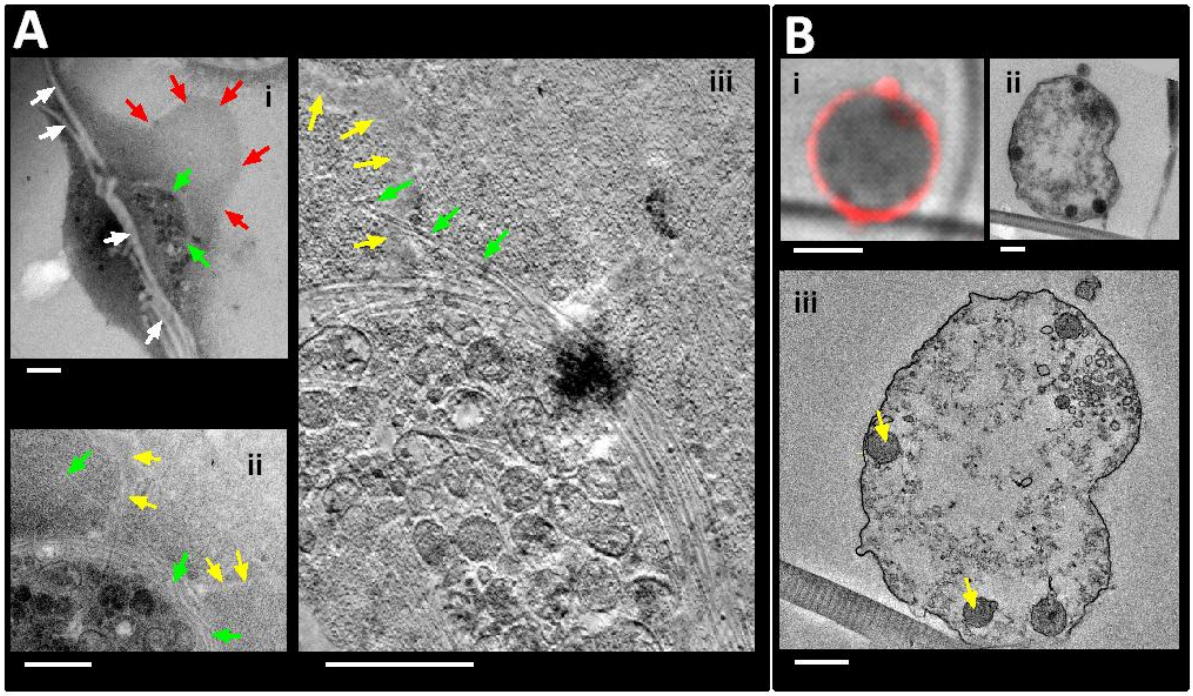

Figure S4: Platelet ballooning involves microtubule disruption at the exit point of the protrusion; related to Figure 5. (A) Transmission electron microscopy of a ballooning human platelet (A-ii and A-iii are zoomed-in views of A-i and A-ii, respectively). A tomogram video file of (A-iii) is provided as Supplementary Movie 8. Green arrows in A point to unwinding microtubules; white arrows point to collagen fibre, red arrows point to balloon membrane, and yellow arrows point to a 'neck-like' structure in the ballooning region of the platelet. (B) Correlative light-electron microscopy of a ballooned platelet. Phase-contrast overlay with annexin-V (in red) (B-i) and transmission electron microscope image (B-ii) of a platelet at Ph_3 (B-iii is zoomed-in view of B-ii)**.** Yellow arrows point to cristae within mitochondria. Scale bar: 1 µm (A-i), 500 nm (A-ii,iii), 2 µm (B-i), 500 nm (B-ii, iii). Data was obtained from platelets analysed from 4 human donors.

SUPPLEMENTARY MOVIES

Movie S1

Platelet membrane ballooning is a consequence of adhesion to collagen; related to Figure 2. Confocal phase contrast images of human platelet adhering to fibrillar collagen were captured at the rate of 1 frame per 4 seconds. Confocal images were acquired using a Perkin Elmer Ultra-VIEW ERS 6FE confocal. Movie was created at 24 frames per second using Volocity 6.3 software.

Movie S2

Membrane balloon increases platelet procoagulant surface; related to Figure 2. Movie is a 3D visualisation of a ballooned human platelet, showing copious accumulation of annexin-V (in red) on both platelet body and inflated/ballooned membrane. Images were acquired by Perkin Elmer Ultra-VIEW ERS 6FE confocal system. Rotated 3D reconstruction of image sections was performed as described in methods using Volocity 6.3 software.

Movie S3

Spatio-temporal dynamics of the early procoagulant response associated with collagen induced human platelet ballooning; related to Figure 2. Fluo-4 (in green) and annexin-V (in red) were used to monitor calcium mobilisation and membrane exposure of phosphatidylserine in real time, respectively. Images were captured as described in methods at a frame per 4 seconds, using a Perkin Elmer Ultra-VIEW ERS 6FE confocal system. Movie was created at 24 frames/second using Volocity 6.3 software.

Movie S4

Ballooned and procoagulant-spread (BAPS) platelets are a distinct subpopulation of human platelet on collagen sites; related to Figure 3. Fluo-4 (green) and annexin-V (red) were used to label intracellular calcium and externalised phosphatidylserine. A z-axis view is shown as image acquisition mode is switched from phase contrast to fluorescence mode. Images were captured at a frame per 4 seconds, using a Perkin Elmer Ultra-VIEW ERS 6FE confocal system. Video rendition was done using Volocity 6.3 software.

Movie S5

Ballooning and procoagulant-spreading visualised (X-Y) orientation; related to Figure 4. A 4-dimensional (4-D: xyz-t) reconstruction of human platelets adherent on collagen shows real time membrane dynamics in the X-Y axis. Images were captured using a Perkin Elmer Ultra-VIEW ERS 6FE confocal system. Images are superimposed annexin-V (red) and $DIOC_6$ (green) 3D re-constructions at selected time-points previously indicated. Movie was created using Volocity 6.3 software.

Movie S6

Ballooning and procoagulant-spreading visualised in (X-Y-Z) orientation; related to Figure 4. A 4-dimensional (4-D: xyz-t) reconstruction of human platelets adherent on collagen showing real time membrane dynamics in the X-Y-Z axis. Images were captured using a Perkin Elmer Ultra-VIEW ERS 6FE confocal. Images are superimposed annexin-V (red) and $DIOC_6$ (green) 3D re-constructions at selected time-points previously indicated. Movie was created using Volocity 6.3 software.

Movie S7

Actin localisation in ballooned and procoagulant-spread platelets; related to Figure 5. Actin was visualised by Alexa Fluor® 350 Phalloidin staining (magenta), intracellular calcium by Fluo-4 (green) and phosphatidylserine exposure by annexin-V (red). Images were captured using a Perkin Elmer Ultra-VIEW ERS 6FE confocal system. Movie was created using Volocity 6.3 software.

Movie S8

Platelets' microtubule bundles disruption is associated with membrane ballooning related to Figure 5. Transmission electron microscopy images were acquired on an Eagle 4k x 4k CCD camera attached to an FEI Tecnai 20, 200kV BioTwin Spirit**.** Movie is a reconstructed single-axis tomogram showing microtubule disruption during active platelet ballooning.

Movie S9

Characteristic membrane retraction of acetazolamide pre-treated human platelet on collagen; related to Figure 7. Annexin-V (red) membrane binding was used to monitor procoagulant activity. Fluo-4 (green) was used to monitor cytosolic calcium. Time-lapse images were captured as described in methods at a frame per 4 second, using a Perkin Elmer Ultra-VIEW ERS 6FE confocal system. Movie was created at 24 frames/second using Volocity 6.3 software.

Movie S10

Membrane balloon collapse in human platelet on collagen, under hyperosmolar challenge; related to Figure 7. Annexin-V (red) membrane binding was used to monitor procoagulant activity. Time-lapse images were captured at the rate of 1 frame per 4 seconds, using a Perkin Elmer Ultra-VIEW ERS 6FE confocal system. Movie was created at 24 frames/second using Volocity 6.3 software.

Coordinated Membrane Ballooning and Procoagulant-Spreading in Human Platelets

Ejaife O. Agbani, Marion T.J. van den Bosch, Ed Brown, Christopher M. Williams, Nadine J.A. Mattheij, Judith M.E.M. Cosemans, Peter W. Collins, Johan W.M. Heemskerk, Ingeborg Hers and Alastair W. Poole

Circulation. published online September 1, 2015;
Circulation is published by the American Heart Association, 7272 Greenville Avenue, Dallas, TX 75231

Print ISSN: 0009-7322. Online ISSN: 1524-4539